Cellulose (2024) 31:4627–4644
https://doi.org/10.1007/s10570-024-05867-z

ORIGINAL RESEARCH

# Facile fabrication of durable and breathable superhydrophobic cotton fabric for self-cleaning, UV-blocking, anti-icing, and photothermal de-icing

**Hua-Bin Yuan · Manman Zhao · Xiaowei Zhu · Desheng Sha · Guoqiang Chen · Tieling Xing**

Received: 16 October 2023 / Accepted: 17 March 2024 / Published online: 12 April 2024


**Abstract** Numerous techniques for achieving superhydrophobic modification of cotton fabrics are documented in existing literature. However, pursuing multifunctionality, especially concerning textile performance, remains a topic of significant research interest. This study introduced a straightforward yet highly effective method for producing modified cotton fabric (SFC) exhibiting a vibrant orange-yellow coloration, along with exceptional self-cleaning, stain-resistant, UV-blocking, anti-icing, and photothermal de-icing properties, through the utilization of ferric chloride hexahydrate ($FeCl_3{\cdot}6H_2O$) and polydimethylsiloxane (PDMS). The surface of the SFC was evenly coated with small nanoparticles, identified by X-ray diffractometer (XRD) as β-FeOOH. The SFC displayed a water contact angle of 165.9° and a sliding angle of 2°, demonstrating outstanding superhydrophobicity. In addition, the SFC achieved a UPF value of 80, indicating exceptional UV-blocking capabilities. Additionally, the SFC exhibited remarkable stability when subjected to harsh conditions, including exposure to strong acid (pH = 1) and alkali (pH = 13), various chemical reagents, 600 min of water washing, and 30 cycles of abrasion testing. The approach proposed in this study offers the advantages of cost-effectiveness, environmental friendliness, and fluorine-free characteristics, and is applicable across a range of fabrics, and has certain practical utility.

**Keywords** Cotton fabric · Superhydrophobic · Self-cleaning · UV-blocking · Photothermal de-icing

## Introduction

Cotton fabric has been widespread due to its comfort, eco-friendly nature, and renewable characteristics (Guo et al. 2020). However, cotton products also have inherent flaws, such as being prone to staining and poor ultraviolet protection ability. Moreover, cotton fabric is prone to freezing in cold regions, leading to diminished insulation and inconvenience for users. With the continuous improvement of living standards and practical needs, consumers are no longer satisfied solely with the privacy coverage, warmth, and decorative functions provided by cotton products. There is an increasing focus on addressing these issues, driving higher demand for functional cotton products (Liu et al. 2020).

**Supplementary Information** The online version contains supplementary material available at https://doi.org/10.1007/s10570-024-05867-z.

H.-B. Yuan · M. Zhao · X. Zhu · D. Sha · G. Chen · T. Xing (✉)
College of Textile and Clothing Engineering, Jiangsu Engineering Research Center of Textile Dyeing and Printing for Energy Conservation, Discharge Reduction and Cleaner Production (ERC), Soochow University, Suzhou 215123, China
e-mail: xingtieling@suda.edu.cn

The self-cleaning and anti-fouling properties of cotton fabrics primarily rely on the presence of superhydrophobic surfaces. These surfaces are achieved by combining surface roughness and low surface energy substances (Wu et al. 2016). Based on this, studies have been reported on combining various nanoparticles with low surface energy substances for superhydrophobic modification of cotton fabrics. For instance, combining silver nanoparticles and polydimethylsiloxane (PDMS) has proven effective in providing cotton fabrics with excellent superhydrophobic, photothermal, and ultraviolet protection properties (Pakdel et al. 2023). However, the high cost and potential safety concerns associated with silver nanoparticles hinder the widespread adoption of this method. Another approach involves using silica particles in combination with (heptadecafluoro-1,1,2,2-tetradecyl) trimethoxysilane, which has been shown to impart superhydrophobic properties to cotton fabrics (Zhang et al. 2012).

Additionally, recent reports have explored the use of new materials such as metal–organic frameworks and *1H,1H,2H,2H*-perfluorooctyltriethoxysilane for superhydrophobic modification of cotton fabrics (Li et al. 2022). These modified cotton fabrics exhibit outstanding self-cleaning and stain-resistant properties. However, it is important to note that the strong chemical resistance of long-chain fluorinated agents raises concerns regarding potential environmental and health risks (Zhao et al. 2016). Fatty acids and bio waxes have emerged as alternatives for low-surface energy substances. However, the durability of hydrophobic coatings prepared from them remains an ongoing challenge (Bayer 2020).

In addition to the nanoparticles mentioned above, FeOOH is undoubtedly an excellent candidate material for superhydrophobic modification due to its low-cost preparation. Over the past decade, various FeOOH nanomaterials have been employed for superhydrophobic applications. For example, β-FeOOH and hydrophobic radicals were utilized to modify copper mesh for superhydrophobicity (Li et al. 2021b). Additionally, β-FeOOH, bayberry tannin, and 1-dodecanethiol were combined to achieve superhydrophobic modification of foams (Chen et al. 2018), while γ-FeOOH and polydopamine were used to prepare multifunctional silk fabrics with superhydrophobicity (Zhou et al. 2020a). Furthermore, FeOOH, particularly β-FeOOH, has been explored for superhydrophobic modification of cotton fabrics. For instance, Cheng et al. pretreated cotton fabric with polydopamine facilitated in-situ growth of β-FeOOH nanorods and treated the fabric with 1-dodecanethiol to achieve excellent superhydrophobic performance. Moreover, Li et al. connected cotton fabric with β-FeOOH using diazotization chemistry, and by controlling the morphology of β-FeOOH, they obtained modified cotton fabrics with different static water contact angles (Li et al. 2021a). While these studies demonstrate the feasibility of improving the superhydrophobic performance of cotton fabrics by introducing FeOOH onto their surfaces, it is important to address some existing issues. For example, the preparation of β-FeOOH often requires high temperature, high pressure, or prolonged hydrothermal methods. Moreover, some modification processes involve additional additives such as urea and dopamine to assist in the growth process, making them time-consuming, energy-intensive, and cumbersome. Additionally, it is crucial to recognize that the reported superhydrophobic modification of cotton fabrics with β-FeOOH primarily focuses on oil–water separation, neglecting other functional aspects. For materials like cotton fabrics, it is of greater significance to endow them with breathability, UV protection, anti-icing, and de-icing properties and applications.

To address the above issues, this work presents a simple and environmentally friendly method for preparing durable and multifunctional superhydrophobic cotton fabric. The unique characteristics of ferric chloride hexahydrate ($FeCl_3 \cdot 6H_2O$) were utilized to produce nanoparticles (β-FeOOH) through hydrolysis. These resulting β-FeOOH nanoparticles were uniformly and densely deposited onto cotton fabric in a single step, providing surface roughness, imparting a bright orange-yellow color to the material, and forming a stable bond with the fabric. Additionally, PDMS was employed to introduce low surface energy substances. The outcome of this process was a multifunctional cotton fabric (referred to as SFC) with distinctive features such as self-cleaning, anti-fouling, UV-blocking, bright coloration, anti-icing, photothermal de-icing, and oil/water separation capabilities. This approach represents a significant advancement in developing multifunctional and durable superhydrophobic cotton fabric.

Furthermore, the multifunctional cotton fabric (SFC) developed in this study demonstrated

outstanding washability, abrasion resistance, breathability, and stability even in extreme environments. The method described in this work is cost-effective but also straightforward and user-friendly. The research provides innovative insights into the production of multifunctional cotton fabrics, and the resulting modified materials hold immense potential for applications in a wide range of fields. It includes but is not limited to outdoor clothing, raincoats, hiking shoes, backpacks, tents, and umbrellas. The multifunctional properties of SFC make it an ideal choice for products that require durability, weather resistance, and enhanced performance in various outdoor and environmental conditions.

## Experimental section

### Materials

Cotton fabric (twill weave, weighing 108 $g \cdot m^{-2}$) was bought from the market. Iron chloride hexahydrate ($FeCl_3 \cdot 6H_2O$, 97.0%) was obtained from Shanghai Lingfeng Chemical Reagent Co., Ltd., China. N, N-Dimethylformamide (DMF, 99.5%), dichloromethane (DCM, 99.5%), cyclohexane (CYH, 99.7%), methanol (MeOH, 99.5%), chlorobenzene (CB, 99.5%), carbon tetrachloride (CTC, 99.5%), tetrahydrofuran (THF, 99.9%), ethanol (EtOH, 99.7%), ethyl acetate (EAC, 99.8%), *n*-heptane (HEP, 98.5%), hexane (HEX, 97.0%), epichlorohydrin (ECH, 99.0%), ammonia water ($NH_3 \cdot H_2O$, 25.0–28.0%), and sodium hydroxide (NaOH, 96.0%) were provided by Jiangsu Qiangsheng Chemical Co. Ltd., China. Polydimethylsiloxane (PDMS, Sylgard 184A) and curing agent (Sylgard 184B) were purchased from Dow Corning Corporation, USA. Oil Red O, Rhodamine B (RhB, 99.0%), Methylene Blue (MB, 98.0%), hydrochloric acid (HCl, GR), and sodium chloride (NaCl, 99.5%) were bought from Shanghai Aladdin Biochemical Technology Co., Ltd., China. All chemicals were analytical grade and were not purified.

### Preparation of SFC

In a conical flask, 2 g of $FeCl_3 \cdot 6H_2O$ was completely dissolved in 50 mL of deionized water. Subsequently, a clean cotton fabric (5×5 cm) was immersed. The flask was then placed in an oscillating dyeing machine, and the temperature was gradually raised to 90 °C. After maintaining continuous oscillation for 1 h, the cotton fabric was removed, washed thrice with deionized water, and dried in an oven. The treated cotton fabric was named FC.

Soon afterward, the FC was immersed in a 50 mL *n*-heptane solution of PDMS (PDMS 0.25 g, Sylgard 184B 0.025 g) for 5 min. Subsequently, the cotton fabric was removed and dried in an 80 °C oven for 3 h. The superhydrophobic cotton fabric was finally obtained and was named SFC.

### Characterization

Scanning electron microscopy (SEM, Hitachi S-8100, Hitachi High Technologies, Japan) with an accelerating voltage of 5 kV was used to investigate the surface micro-topography. Before testing, the sample pasted on the conductive adhesive was pre-sprayed with platinum to increase conductivity. ATR-FTIR (Nicolet 5700, Thermo Fisher Scientific, USA) and X-ray photoelectron spectrometer (XPS, ESCALAB 250Xi, Thermo Fisher Scientific, USA) were served to analyze the molecular structure and chemical composition. An X-ray diffractometer (XRD, Rigaku Ultima IV, Rigaku Corporation, Japan) with a D/tex Ultra detector was used to characterize crystallinity and structure. The diffractometer employed a Cu Kα X-ray source with a wavelength of 1.5406 Å. The scan rate was set at 2°/min while the 2θ angle of the diffractometer was stepped from 5° to 50°. Before testing, the sample size of 2×2 cm pasted on the plasticine was fixed to the sample slot. An atomic force microscopy (AFM, VEECO Multimode 8, Bruker) was used to measure the surface roughness. The measurement was conducted in tapping mode with a sample size of 1×1 cm. The scan range was set at 3×3 μm. The probe (BRUKER, model: SCANASYST-AIR) had a triangular cantilever with a rigidity of 0.4 N/m. A fully automatic multifunctional color difference instrument (UltraScan PRO, Hunter Lab, USA) was utilized to test the K/S value of samples. The sample was folded twice during the test, and the average K/S value of the four areas on the sample was used as the final result. A Krüss DSA 100 instrument (DSA 100, Krüss, Germany) was served to characterize the static water contact angle (CA) with deionized water (6 μL). This device also measured the sliding angle (SA), and the volume of

the droplets was 10 μL. Each sample was tested three times by selecting three points from various regions, and the final result was obtained by averaging the measurements.

Washing resistance test

The washability test was performed following the ISO105-C10:2006 standard. A 5×5 cm sample was immersed in a standard washing solution with a concentration of 5 g·$L^{-1}$ (bath ratio 1:50). Then, the speed was set as 40 rpm, and the temperature was set as 40 °C. At intervals of 30 min, the sample was removed, marking the completion of each washing cycle. The contact and sliding angles were measured after washing 3 times with deionized water and drying at room temperature.

Abrasion resistance test

The abrasion resistance test comprised the following steps. Initially, the sample was positioned on a 1000 mesh sandpaper, with a 100 g weight applied. The weight was then pulled back and forth, exerting a force at a speed of 1 cm/s, covering a distance of 10 cm. Then, the sample was removed and designated as completing one abrasion cycle. Subsequently, the CA and SA were measured.

Chemical stability tests

The stability test included the following steps. Firstly, the sample was immersed in different solutions for 24 h, including HCl solution (pH = 1), HCl solution (pH = 4), NaCl solution (pH = 7), NaOH solution (pH = 10), NaOH solution (pH = 13) and different organic solvents (DMF, DCM, CYH, MeOH, CB, CTC, THF, EtOH, EAC, HEP, HEX). Subsequently, the sample was removed and washed with ethanol three times. After drying at room temperature, the CA and SA were tested.

UV-resistance test

A UV transmittance analyzer (UV-2000, Labsphere, USA) was used to test the UV-resistance property. All the samples were tested five times, and the average value was taken as the final result.

Oil/water separation measurements

The oil/water separation test included the separation of heavy oil and water mixtures and the separation of light oil and water mixtures, which were separated using self-made separation devices. For ease of observation, oil and water were stained with Oil Red O and MB, respectively. The volume of oil and water was both 50 mL. After separation, the volume of oil was collected and measured, and the separation efficiency was calculated according to Eq. (1) (Ahmad et al. 2023).

$$\eta = \frac{V_1}{V_0} \times 100 \tag{1}$$

where, $\eta$ is separation efficiency, $V_0$ and $V_1$ are the volumes of oil before and after separation, respectively.

The permeation flux was calculated according to Eq. (2) (Xie et al. 2023).

$$J = \frac{V}{st} \tag{2}$$

where, $J$ (L·$m^{-2}$· $h^{-1}$) is the permeation flux, $V$ (L) is the volume of collected oil, $s$ ($m^2$) is the effective separation area, and $t$ (h) is the time required to complete the separation.

Anti-icing test

The anti-icing performance was assessed using a custom-built apparatus comprising a low-temperature cooling device (DKB 2410, Jinghong instrument and equipment Co., Ltd., China), a high-speed camera, and a multi-channel temperature recorder (LIANYI SH-16XL, Dongguan, China). During the testing process, the test sample was initially placed on the cooling platform set at a temperature of -20 °C. Subsequently, 10 μL of water droplets were deposited onto the sample surface, and the temperature and morphology changes of the water droplets were recorded.

Photothermal conversion and de-icing tests

The photothermal conversion and de-icing performance of the samples were assessed utilizing custom-designed equipment. For the photothermal conversion test, the sample was placed flat on the workbench

and subjected to xenon lamp illumination to simulate natural light (PLS-SXE300+, Beijing, China). The temperature variations were monitored and recorded using a multi-channel temperature recorder (LIANYI SH-16XL, Dongguan, China).

In testing the photothermal de-icing performance, the sample was placed on a cooling platform and allowed to reach thermal equilibrium in a -20 °C environment for 10 min, ensuring that the sample surface temperature aligned closely with the ambient temperature. Following this, 50 µL water was added to the sample surface to freeze into ice in the -20 °C environment. Subsequently, various irradiation intensities from the xenon lamp light source were employed for illumination. The melting process of the ice and the temperature were recorded using the multi-channel temperature recorder and a camera.

## Results and discussion

### Surface morphology and roughness

Figure 1a, b, c illustrate the surface microstructure of the original cotton fabric, SFC, and SFC at high magnification, respectively. The electron microscope images revealed that the surface of the original cotton fabric appeared smooth, consistent with previous literature findings (Cheng et al. 2019). However, it was observed that dense particles were firmly attached to the surface of SFC, significantly enhancing the surface roughness of the cotton fabric.

AFM was used to characterize both the original cotton and SFC to assess the increase in surface roughness. The scanning area was 3×3 µm. The corresponding results are displayed in Figs. S1 (a, b). The average roundness ($R_a$) of raw cotton was 13.1 nm, and the root mean square roundness ($R_q$) was 17.8 nm. Despite slight undulations on the surface of the natural cotton, it remained relatively smooth, aligning with the SEM results. In contrast, the $R_a$ of SFC was 46.5 nm, and the $R_q$ was 65.5 nm. Compared with the original cotton, it is evident that the surface roughness of SFC significantly increased, thereby enhancing the hydrophobicity of the cotton fabric (Sharma et al. 2023).

### Chemical compositions

As shown in Fig. 2a, FTIR-ATR spectroscopy was used to analyze the changes in functional groups. The absorption peak at 3331 $cm^{-1}$ was attributed to –OH in cellulose (Chen et al. 2019). The peak that appeared at 2894 $cm^{-1}$ was caused by the stretching vibration of the $-CH_2$ group in cellulose (Chung et al. 2004). The spectrum of FC did not exhibit any significant changes compared to the original cotton fabric. After undergoing further processing by PDMS, three distinct new peaks appeared in the spectrum of SFC, located at 2962 $cm^{-1}$, 1260 $cm^{-1}$, and 801 $cm^{-1}$, respectively. The peak at 2962 $cm^{-1}$ can be attributed to the stretching vibration of $-CH_3$, which was caused by the introduction of PDMS (Chen et al. 2021). The peak at 1260 $cm^{-1}$ corresponded to the deformation vibration of $–CH_3$ in $Si–CH_3$ (Jiang et al. 2022), while the obvious absorption peak at 801 $cm^{-1}$ pertained to the stretching vibration of Si–O–Si (Chung et al. 2004). The emergence of these three fresh peaks demonstrated the successful integration of PDMS on the cotton fabric.

The presence of iron elements in SFC could not be determined from the FTIR-ATR spectrum. Consequently, XPS was employed for further characterization. The XPS full spectrum (Fig. 2b) confirmed the

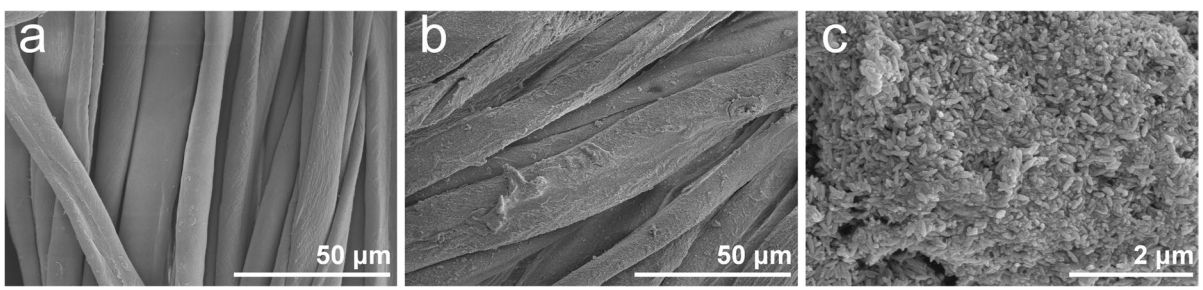


**Fig. 1** SEM morphology images of original cotton (**a**), SFC (**b**), SFC at high magnification (**c**)

presence of iron in SFC. Additionally, the appearance of Si absorption peaks supported the findings obtained from the FTIR-ATR spectrum analysis.

The chemical composition of particles on the surface of SFC was further characterized using XRD, as shown in Fig. 2c. The original cotton exhibited typical crystal planes attributed to cellulose I at 14.87°, 16.7°, and 22.8° (Ling et al. 2019). Some new diffraction peaks appeared in the SFC spectrum, respectively, at 2θ Values were 12.1° (1 1 0), 16.9° (2 0 0), 26.9° (3 1 0), 34.3° (4 0 0), 35.4° (2 1 1), 39.4° (3 0 1), and 46.7° (4 1 1) (Hu and Li 2012). The positions of these peaks were consistent with the simulated values of β-FeOOH (COD-1008768) shown in Fig. 2d. The diffraction peaks corresponded one-to-one, and their appearance confirmed the chemical composition of the particles on the SFC surface were β-FeOOH.

## Wettability

Modifying cotton fabric by $FeCl_3 \cdot 6H_2O$ and PDMS achieved superhydrophobic properties, as shown in Fig. 3a. The original cotton fabric had a CA of 0°. In contrast, the modified SFC displayed a CA of 165.9° and a sliding angle 2°. In Fig. 3b, the partially submerged SFC exhibited the silver mirror phenomenon under the water surface. The rough surface structure of the fabric allowed air to accumulate, forming a luminescent silver mirror due to light illumination (Gu et al. 2022). Furthermore, in Fig. 3c, various droplets, including water, RhB solution, MB solution, tea, soy sauce, and hot water, maintained spherical shapes on the SFC surface after 30 min, demonstrating stable contact angles. When the SFC was erected, these droplets immediately rolled off without leaving any noticeable trace (Fig. 3d), indicating low water adhesion of the SFC (Shang et al. 2021). Conversely, SFC was observed to be lipophilic; upon contact with an oil drop, it immediately became wetted.

As depicted in Fig. 3e and Video S1, a continuous stream of water was fired from a syringe onto the SFC surface, where it changed direction and bounced off at an angle without leaving any stains on the SFC surface. These observations indicate the excellent superhydrophobic properties and splash resistance of SFC (Liu et al. 2023).

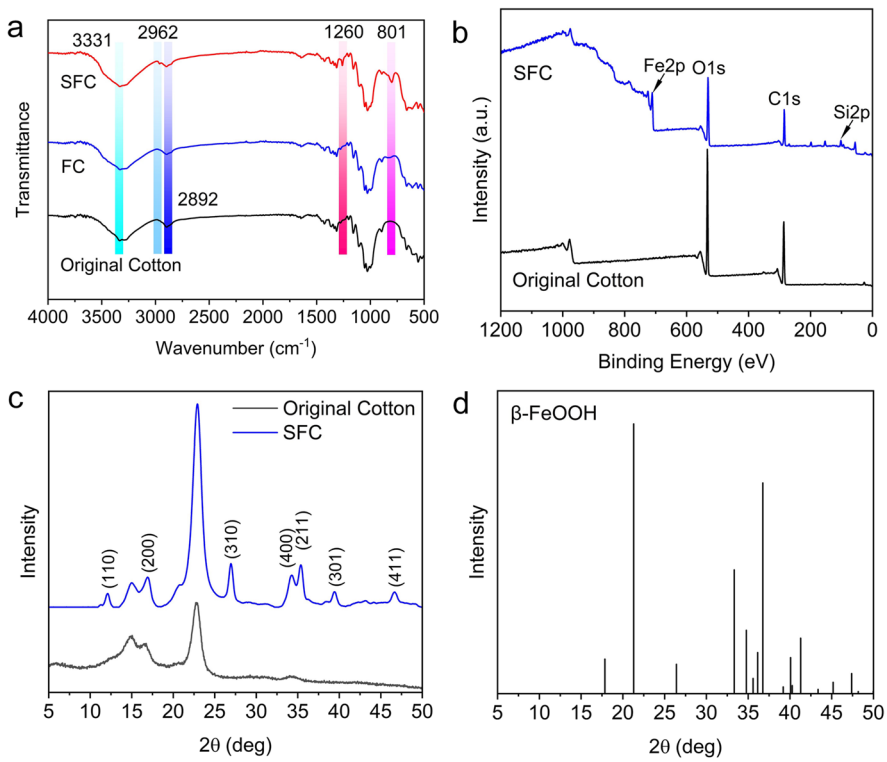


**Fig. 2** Infrared spectra of original cotton, FC, and SFC (**a**); XPS (**b**) and XRD (**c**) spectra of original cotton and SFC; simulated XRD spectra of β-FeOOH (**d**)

Anti-fouling and self-cleaning performance

In our daily lives, it is not uncommon to accidentally splatter liquids like ink, fruit juice, or red wine onto our clothing. Such incidents can easily cause staining and contamination of the fabric. Therefore, evaluating the anti-fouling performance of superhydrophobic modified cotton fabrics becomes crucial (Yang et al. 2023).

The anti-fouling ability of SFC was tested by immersing in a high-concentration MB solution, as shown in Fig. 4a and Video S2. Even after vigorous stirring within the solution, no traces of residual liquid were observed on the surface of the SFC. Conversely, the original cotton fabric acquired a blue tinge when exposed to the same solution (Fig. 4b and Video S3).

The self-cleaning performance is another vital characteristic that superhydrophobic cotton fabrics should possess. In this study, to demonstrate the exceptional self-cleaning ability of SFC against various pollutants more effectively, several solid pollutants such as MB powder, chalk dust, and carbon powder were chosen. These pollutants were deliberately sprinkled onto the surface of the SFC and then flushed with flowing water. The results are presented in Fig. 5a, b, c, and Videos S(4, 5, 6). It was observed that all three types of impurities were effortlessly and thoroughly removed from the surface of SFC, leaving no residue behind. Such a phenomenon is related to the rough surface structure of SFC. This structure leads to an increased CA on the SFC surface, making water droplets prone to sliding off. When water droplets roll on the surface, they carry away surface contaminants or dust, achieving a self-cleaning effect.

It was evident that SFC exhibited outstanding anti-fouling and self-cleaning performance from these results presented in Figs. 4 and 5.

Chemical and durability stability

The durability and chemical stability of SFC are illustrated in Fig. 6. Figure 6a depicts the alterations in CA and SA of SFC following immersion for 24 h in HCl solution (pH = 1), HCl solution (pH = 4), NaCl solution at (pH = 7), NaOH solution (pH = 10), and NaOH solution (pH = 13). As evident from the diagram,

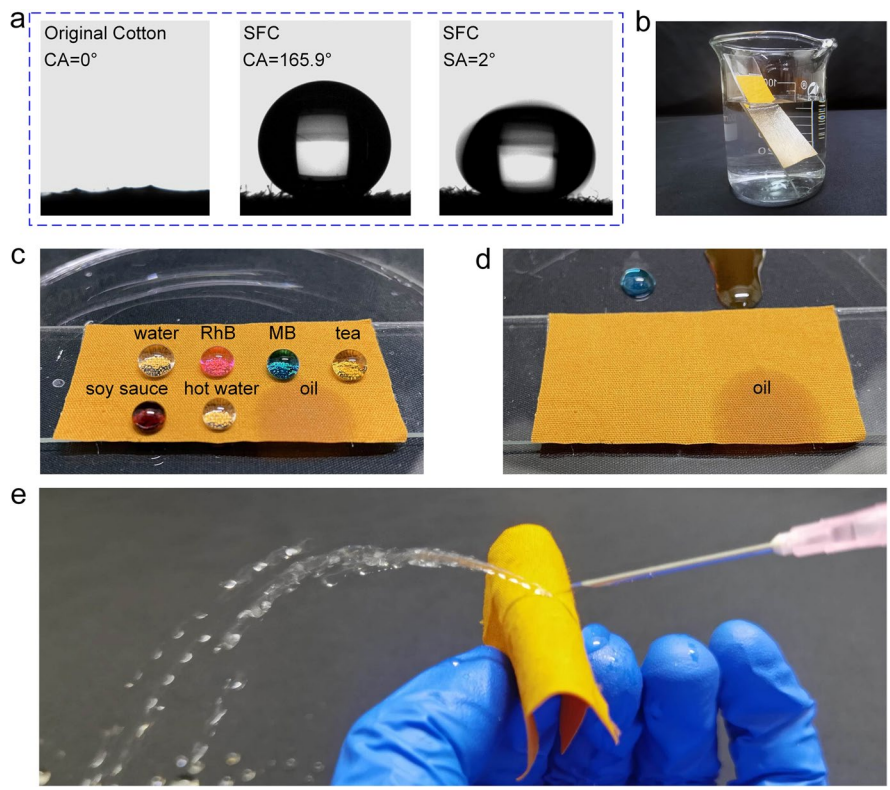


**Fig. 3** CA of original cotton, CA and SA of SFC (**a**); silver mirror phenomenon of SFC (**b**); wettability of different droplets on SFC surface (**c**, **d**); a continuous stream of water flow rebounded on SFC surface (**e**)

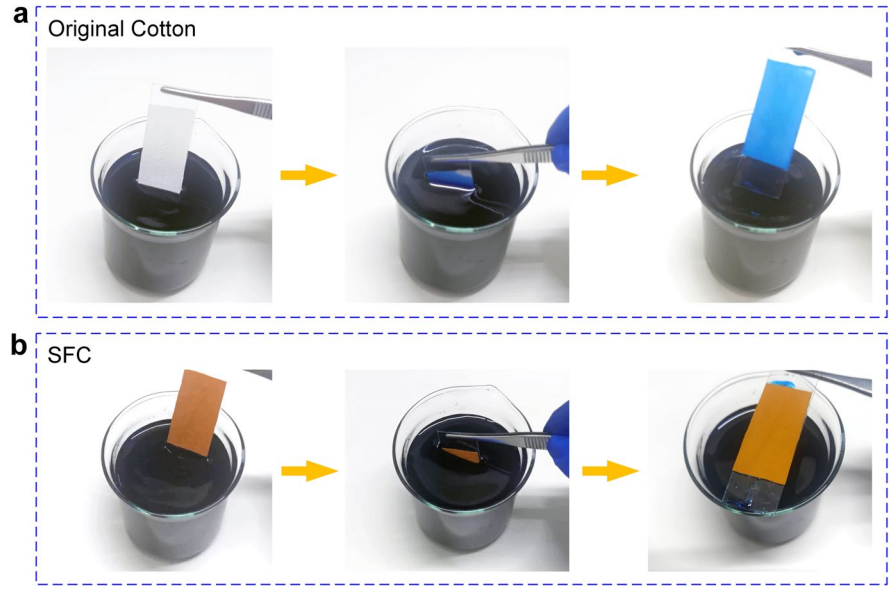


**Fig. 4** Original cotton (**a**) and SFC (**b**) immersed in high-concentration MB solution

there was only a minor reduction in the CA of SFC under all circumstances, while its SA remained below 8°. These findings suggest that SFC can maintain excellent superhydrophobic performance even when exposed to extreme pH conditions (such as pH = 1 and pH = 13), ensuring its stability in different chemical environments. Figure 6b presents the changes in CA and SA of SFC after soaking in various organic solvents for 24 h. The graph reveals that certain organic solvents, such as methanol (MeOH), chlorobenzene (CB), tetrahydrofuran (THF), and ethanol (EtOH), significantly impacted the superhydrophobic properties of SFC, while other solvents had minimal effect. Nonetheless, even after soaking SFC in these solvents for 24 h, its CA remained above 150°, while its SA was still below 10°, demonstrating its outstanding superhydrophobic performance. These results indicate that SFC exhibits remarkable stability under different chemical environments.

Figure 6c illustrates the changes in the superhydrophobic performance of SFC after undergoing standard washing for 600 min. The results show that with the prolongation of washing time, the CA of SFC exhibited a gradual decline, while the SA displayed a gradual increase. Nonetheless, even after being washed for 600 min, the CA of SFC remained above 150°, and its SA remained below 8°, indicating its superb washing resistance. To further demonstrate the outstanding wash stability of the SFC, we conducted tests on the CA variation of the SFC with increasing washing speeds (45 rpm, 50 rpm) over time (Fig. S2). It was observed that as the washing speed increased, the CA of the SFC exhibited a decreasing trend. However, even after continuous washing for 600 min at a speed of 50 rpm, the CA of the SFC remained close to 150°. Additionally, Fig. S3 presents the influence of washing speed on the surface morphology of the SFC. Compared to the unwashed SFC, the surface of the SFC subjected to different washing speeds only exhibited some loss of loosely bound β-FeOOH particles, while the overall rough structure remained relatively intact. These results effectively demonstrate the excellent wash stability performance of the SFC.

In Fig. 6d, the durability of SFC is demonstrated after experiencing repeated abrasion on sandpaper. As the abrasion times increased, the CA of SFC showed a decreasing trend. However, even after 30 abrasion cycles, the SFC still maintains its superhydrophobic performance. The decline in CA during the initial stage of abrasion cycles (0–10 cycles) is rapid, followed by a slower decline during cycles 10–20 and a gradual decrease as the cycles continue to increase. The stepped change can be attributed to the severe abrasion of the superhydrophobic coating on the SFC surface at the beginning, leading to damage to the cotton fibers

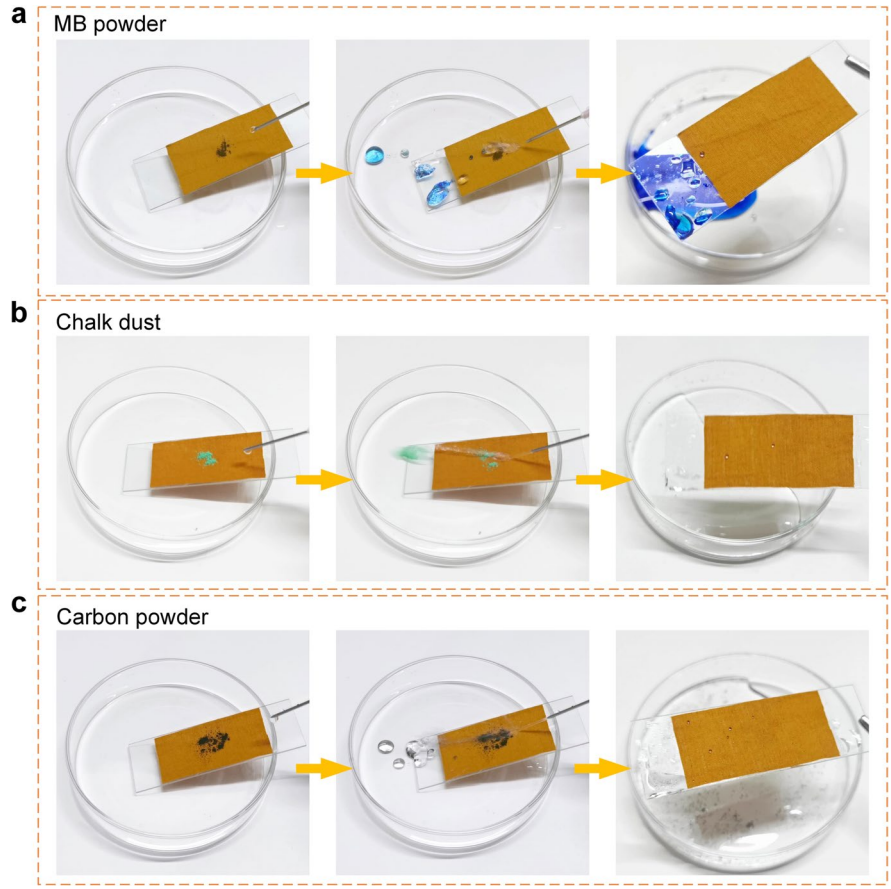


**Fig. 5** Self-cleaning test of SFC by using different contamination (**a** MB powder, **b** chalk dust, **c** carbon powder)

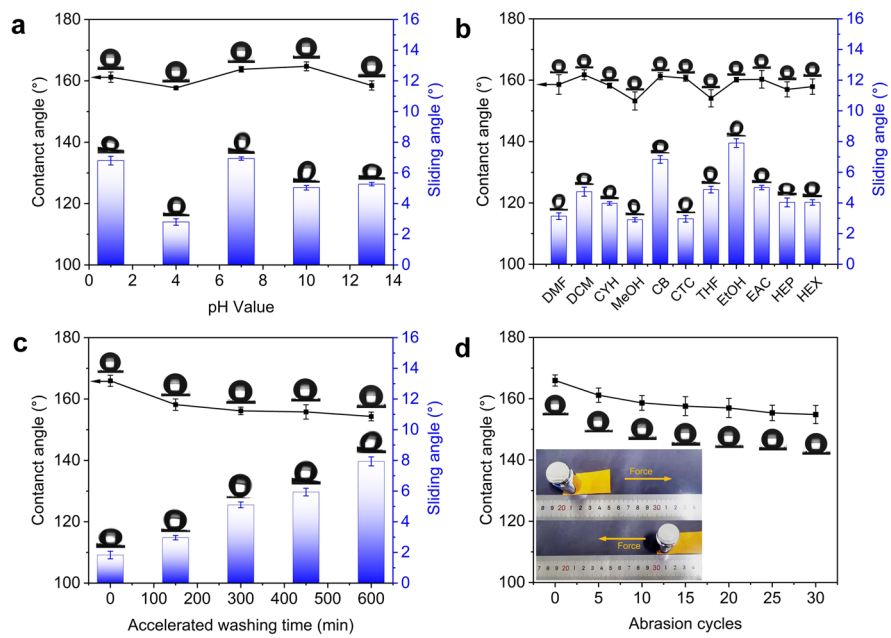


**Fig. 6** Changes in the CA of SFC after immersion in solutions with different pH values (**a**) and different organic solvents (**b**) for 24 h; effect of washing time (**c**) and abrasion cycles (**d**) on the CA of SFC

and an increase in surface roughness (as indicated in Fig. S4). As the abrasion cycles further increase, the enhanced roughness is no longer sufficient to maintain the declining trend of CA (Zhou et al. 2018).

The strong stability of SFC was tested according to the GB/T 3923.1–2013 standard, and the results are shown in Fig. S5. Compared to the original cotton fabric, both the breaking strength and breaking elongation of SFC decreased, which could be attributed to the high-temperature treatment during the modification process.

The outcomes depicted in Fig. 6 demonstrate that SFC exhibits outstanding chemical stability and durability, suggesting its potential for application under diverse extreme conditions. These remarkable characteristics of SFC indicate its wide range of practical applications, such as self-cleaning and anti-adhesion coatings, anti-icing surfaces, oil/water separation, and further boosting its chances for widespread usage.

## Breathability

According to previous reports, the breathability of SFC was evaluated by utilizing the reaction between concentrated ammonia water and hydrochloric acid, which produced white smoke during the response (Wang et al. 2020).

The testing procedure involved injecting an appropriate quantity of each substance into two separate glass bottles, which were then tightly sealed. The cap of the bottle containing concentrated hydrochloric acid was then opened, and the mouth of the bottle was promptly closed with SFC. Subsequently, the cap of the glass bottle containing concentrated ammonia water was opened. Due to the high volatility of concentrated hydrochloric acid and concentrated ammonia, the production of white smoke was immediately observed (Fig. 7 and Video S7). Results from this test indicated that even after modification by $FeCl_3{\cdot}6H_2O$ and PDMS, SFC maintained superb breathability, affirming its comfortability and promising practical applications.

## Color feature

Figure 8 and Table 1 show the effect of washing times on the surface color of SFC. From Fig. 8, it can be observed that fewer washing cycles (5 cycles) had a minimal effect on the color of SFC. As the washing frequency gradually increased, the K/S value of SFC exhibited only a slight decrease. The variation pattern of the color feature index shown in Table 1 was also consistent with the results in Fig. 8. These results indicate that SFC has outstanding washability and reflects the application prospects of SFC in fields such as sanitation suits and life jackets.

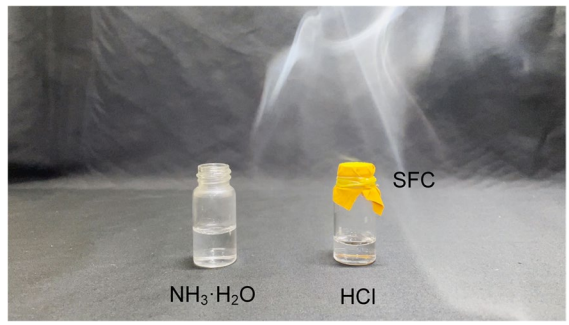


**Fig. 7** Breathability of original cotton fabric and SFC

## Oil/water separation performances

Figure 9 illustrates the separation process and effectiveness of SFC on different oil/water mixtures.

Figure 9a and Video S8 document the SFC separation process of heavy oil and water mixtures. During the test, SFC was fixed between the upper and

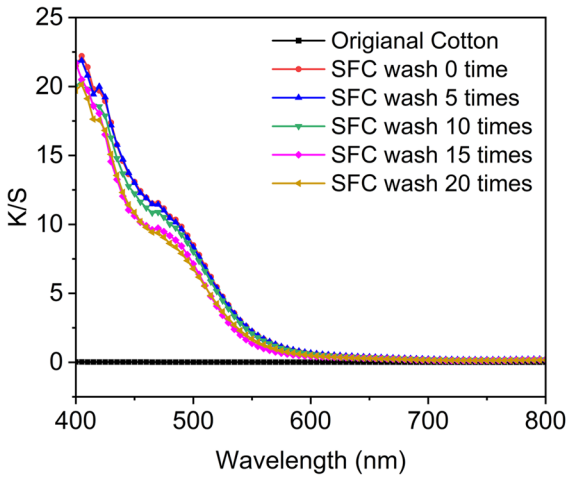


**Fig. 8** Color absorption spectra of cotton fabrics

**Table 1** The effect of washing times on color feature values of cotton fabrics

| Samples | L* | a* | b* | C* | h* |
|---|---|---|---|---|---|
| Original Cotton | 94.34 | -0.31 | 1.89 | 1.92 | 99.13 |
| SFC washed 0 time | 50.053 | 27.01 | 47.76 | 54.86 | 60.52 |
| SFC washed 5 times | 51.03 | 27.11 | 48.24 | 55.34 | 60.68 |
| SFC washed 10 times | 55.46 | 25.25 | 53.43 | 59.09 | 64.71 |
| SFC washed 15 times | 53.66 | 26.49 | 50.21 | 56.77 | 62.19 |
| SFC washed 20 times | 50.28 | 27.72 | 48.26 | 55.66 | 60.13 |

lower glass bottles. SFC effectively and rapidly separated the heavy oil and water under gravity alone. As shown in Fig. 9c, SFC exhibited remarkable separation efficiency for four commonly encountered heavy oils, namely epichlorohydrin (ECH), chlorobenzene (CB), dichloromethane (DCM), and carbon tetrachloride (CTC). The separation efficiencies of these oils were all above 95%. In practical applications, the ability of oil/water separation materials to be recycled is crucial.

For this reason, the mixture of CTC and water was selected as the target for separation. The separation efficiency and permeation flux were evaluated over 30 separation cycles. As depicted in Fig. 9d, the results revealed a hard decrease in the separation efficiency and a significant decline in permeation flux. It could be attributed to the potential blocking of some pores in SFC during continuous separation cycles. Notably, the initial oil permeation flux of SFC for CTC was 34,323 $L{\cdot}m^{-2}{\cdot}h^{-1}$ and remained higher than 10,000 $L{\cdot}m^{-2}{\cdot}h^{-1}$ even after 30 times continuous separations. The separation outcomes highlight the exceptional performance of SFC compared to most reported separation materials based on cotton fabric (as displayed in Table 2).

Moreover, as displayed in Fig. 9b, the separation performance of SFC for light oil and water mixtures was also examined. The separation efficiency for various light oils is exhibited in Fig. 9c. The results indicate that SFC demonstrates outstanding separation efficiency for four light oil and water mixtures: hexane (HEX), *n*-heptane (HEP), ethyl acetate (EAC), and cyclohexane (CYH). Particularly, for the mix of HEP and water, the separation efficiency of SFC reached nearly 99%.

Overall, the findings in Fig. 9 underscore the practical applicability and broad potential of SFC in separating various oil/water mixtures.

## Ultraviolet resistance

Multiple studies have demonstrated that continuous exposure of the human skin to ultraviolet radiation can lead to notable risks, such as skin cancer (Xiong et al. 2020). Clothing, an essential item for humans, can effectively reduce or isolate direct contact with UV rays. Unfortunately, most clothing products today lack adequate UV-blocking capabilities

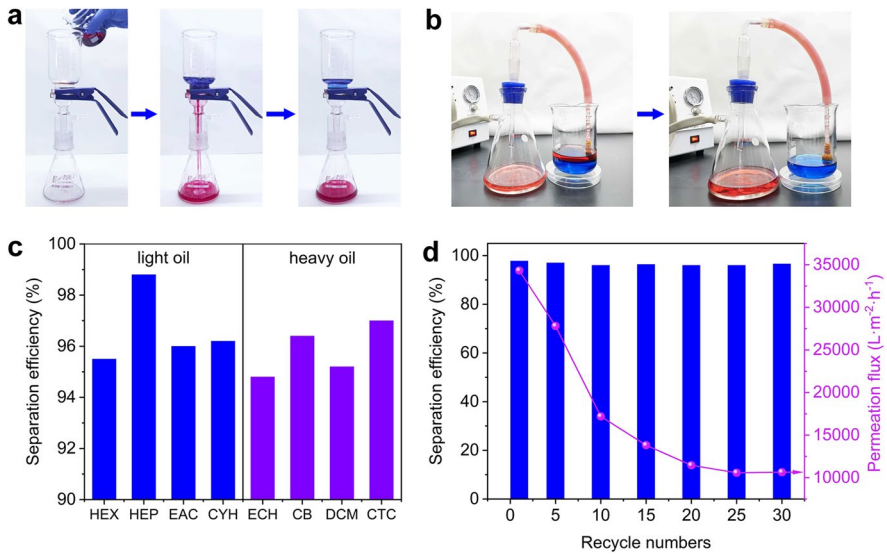


**Fig. 9** SFC used in the separation process of heavy oil and water mixtures (**a**); SFC used in the separation process of light oil and water mixtures (**b**); separation efficiency of SFC for different oil–water mixtures (**c**); effect of cycle times on SFC separation efficiency and oil permeation flux (**d**)

**Table 2** Oil permeation flux of different modified cotton fabrics

| Materials | Organic | Flux ($L \cdot m^{-2} \cdot h^{-1}$) | Reference |
|---|---|---|---|
| β-FeOOH, PDMS | carbon tetrachloride | 34,323 | This work |
| rosin acid, $SiO_2$ | toluene | 7000 | (Chen et al. 2022) |
| tannic acid, polyhedral oligomeric silsesquioxane | toluene | 20,000 | (Shang et al. 2021) |
| ZIF-8, PVDF, PDMS | crude oil | > 15,300 | (Zhang et al. 2022) |
| T-ZnO | xylene | 6092 | (Liu et al. 2022) |
| $TiO_2$, cyanate ester | petrol | 7200 | (Arumugam et al. 2021) |
| N-octylalkoxysilane | benzene | 12,540 ± 146 | (Zhou et al. 2020b) |
| | tetrachloromethane | 13,620 ± 184 | |
| | ethyl acetate | 11,460 ± 113 | |
| | gasoline | 12,900 ± 82 | |
| | edible oil | 11,820 ± 133 | |
| PDA, palmitic acid | *n*-hexane | 3400 | (Mohamed and Abd-El-Nabey 2021) |

(Zhang et al. 2023). Therefore, there is a dire need to develop cotton fabrics that offer UV protection, as they are widely preferred by consumers.

This work used a UV transmission analyzer to evaluate the shielding effect of original cotton and SFC on UV radiation. As displayed in Fig. 10a, the transmittance of UV radiation is shown for original cotton and SFC. It can be observed that the original cotton exhibited a significantly high UV transmittance value of 30%. Conversely, SFC demonstrated an ability to obstruct UV rays, with a transmittance value of less than 2.5%.

Furthermore, Fig. 10b shows the changes in three vital UV-blocking indicators: UPF, UVA, and UVB.

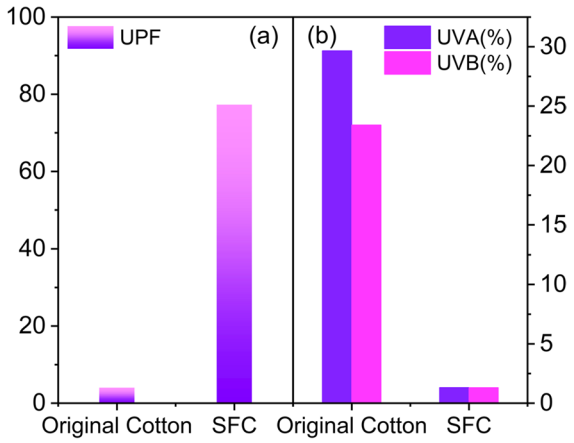


**Fig. 10** Transmittance of UV light from original cotton and SFC (**a**); UPF, UVA, and UVB of original cotton and SFC (**b**)

The original cotton lacked any significant UV insulation capability, with UPF = 4, UVA = 29.7%, and UVB = 23.4%. In contrast, SFC had a UPF value close to 80, while UVA and UVB values were below 1.5%. These results indicate a remarkable improvement in UPF value and a significant reduction in UVA and UVB values for SFC compared to the original cotton. These findings inferred that the introduction of $FeCl_3 \cdot 6H_2O$ and PDMS resulted in forming a UV reflective layer on the surface of cotton fabric, thereby endowing it with excellent UV shielding capability (Emam et al. 2020).

## Anti-icing performance

The anti-icing performance of the original cotton fabric and SFC was evaluated through testing using a custom-built apparatus. Due to the excellent hydrophilicity of the original cotton fabric, our repeated tests showed that the surface water droplets on it froze within 90 s, which is consistent with the results from our previously published literature (Yuan et al. 2024). The delayed icing capability of SFC is presented in Fig. 11. As the testing time extended, the temperature of water droplets on the SFC surface reached 0 °C and continued to decrease, entering a supercooled state. When the temperature of the droplets dropped to -16 °C, they instantly underwent a phase transition. It is observed from the curve shown in Fig. 11, where the temperature of the droplets experiences a

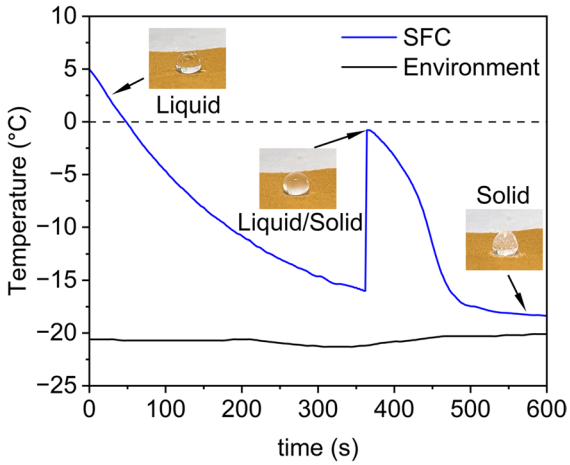


**Fig. 11** Anti-icing performance of SFC

sudden increase to about 0 °C due to the latent heat release. The time consumed by the droplets from 0 °C to the start of the phase transition is defined as the freezing time ($t_i$), and according to Fig. 11, the $t_i$ of SFC is 315 s.

Additionally, it can be observed from Fig. 11 that the phase transition stage of SFC is very short, lasting only 8 s. During this stage, the water droplets on the SFC surface shift from a liquid/solid hybrid state to a solid state until completely frozen, and this period is defined as the freezing time ($t_f$). After the droplets are completely frozen, their shape changes, presenting a peach-like appearance. Therefore, based on the recorded results in Fig. 11, the delayed icing time of SFC is calculated as 323 s ($t_i + t_f$). Compared to the original cotton fabric, SFC exhibits improved delayed icing performance.

The thermal loss of water droplets per unit of time ($\Delta Q$) is mainly related to three factors: the heat transfer at the solid–liquid interface ($Q_c$), the thermal radiation between the droplets and the air cushion ($Q^*_r$), and the convective heat transfer between the droplets and the surrounding air ($Q_r$). Among these factors, $Q_c$ represents the major form of heat loss in this process. $Q_c$ can be calculated based on Fourier's law as shown in Eq. (3):

$$Q_c = \lambda \bullet S_{sl} \bullet \left( \frac{T_w - T_s}{x} \right) \tag{3}$$

where, $\lambda$, $T_w$, $T_s$, $x$, and $S_{sl}$ represent the thermal conductivity of the substrate, the initial temperature of the water droplet, the ambient temperature, the thickness of the substrate, and the effective solid–liquid contact area, respectively.

Due to the air layer between SFC and water droplets, it has a lower $S_{sl}$, resulting in a smaller $Q_c$. It ultimately prolongs the heat dissipation time of water droplets, thereby exhibiting delayed freezing performance (Zhou et al. 2023).

## Photothermal conversion and de-icing

Figure 12a demonstrates the excellent photothermal conversion capability of SFC. As observed from the graph, the surface temperature of SFC increased rapidly with extended exposure time to xenon lamp light. This phenomenon is primarily attributed to the photothermal conversion property of β-FeOOH on the surface of SFC (Żebrowska et al. 2020). Additionally, as the irradiance gradually increased from 0.32 W·cm$^{-2}$ to 0.64 W·cm$^{-2}$, the maximum surface temperature achievable by SFC increased from 70 °C to 110 °C. Upon removal of the light source, the surface temperature of SFC quickly decreased to room temperature. In contrast, the surface temperature of the original cotton fabric only increased by 5 °C after continuous irradiation for 300 s under a simulated light source with an irradiance of 0.48 W·cm$^{-2}$.

Figure 12b presents the cyclic thermal stability of SFC under the irradiation of a simulated light source with an irradiance of 0.48 W·cm$^{-2}$. In each cycle of 60 s light exposure followed by 60 s without light, the surface temperature of SFC reached up to 83 °C. After removing the light source, the surface temperature rapidly decreased to the ambient level. Even after 5 cycles, the photothermal conversion performance of SFC remained stable, indicating its excellent thermal properties.

Moreover, we conducted additional tests on the CA of the SFC after being irradiated for 5 min with simulated light sources at irradiance intensities of 0.32 W·cm$^{-2}$, 0.48 W·cm$^{-2}$, and 0.64 W·cm$^{-2}$ (Fig. S6). Furthermore, we also performed CA measurements on the SFC after undergoing five cycles of continuous irradiation at an intensity of 0.48 W·cm$^{-2}$ (Fig. S7). The results from the figures indicate that the superhydrophobic performance of SFC exhibits favorable photostability performance.

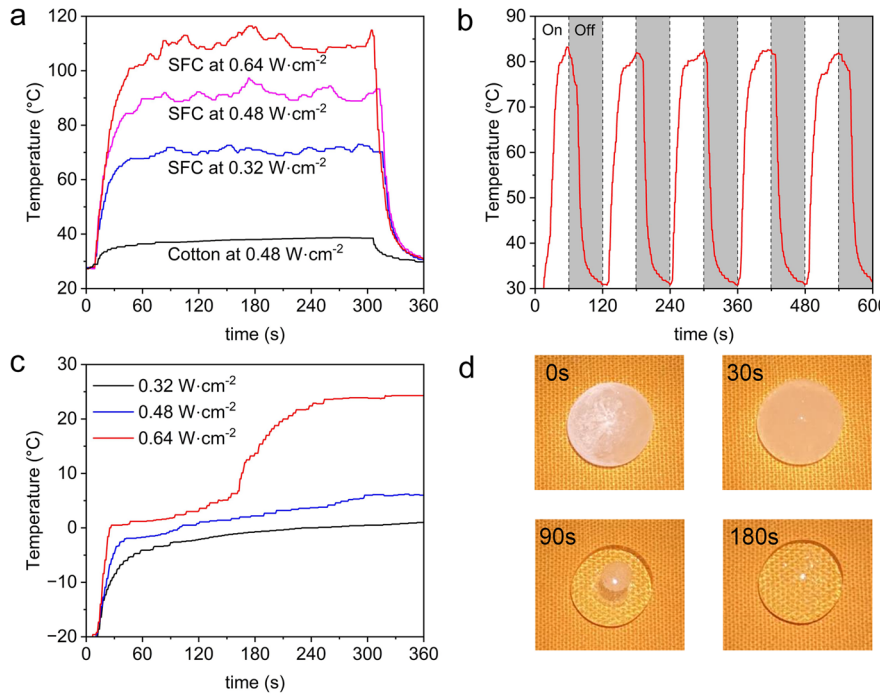


**Fig. 12** The variation of surface temperature between the original cotton fabric and SFC under different irradiation intensities (**a**); the cyclic photothermal conversion capability of SFC (**b**); the variation of ice temperature on the surface of SFC with time under different irradiation intensities (**c**); the state of ice blocks on the surface of SFC at different time points under irradiation intensity of 0.64 W·cm.$^{-2}$ (**d**)

The results depicted in Fig. 12c represent the variation of the ice block temperature on the surface of SFC overtime under the irradiation of a simulated light source with different irradiance levels. At lower irradiance (0.32 W·cm$^{-2}$), the ice block remained partially unmelted within a time range of 360 s, with its temperature consistently below 0 °C. As the irradiance increased to 0.48 W·cm$^{-2}$, the ice block temperature exceeded 0 °C after 180 s of xenon lamp irradiation, indicating the initiation of melting. With further prolonged irradiation, the temperature of the ice block rose to 5 °C. When the irradiance continued to increase to 0.64 W·cm$^{-2}$, the ice block on the surface of the SFC started to melt after 30 s irradiation. In Fig. 12d, the ice block exhibited a mixed solid–liquid state at this point. After 90 s of irradiation, most ice blocks transformed into a liquid phase. After 180 s, the ice block was entirely melted, and the temperature of the liquid droplets reached approximately 15 °C. It is noteworthy that due to the superhydrophobic property of SFC, the liquid droplets formed after ice melting cannot wet the surface of SFC. The droplets could swiftly slide off the surface when SFC was held upright. The test results presented in Fig. 12c, d demonstrate the outstanding ice removal performance of SFC using photothermal conversion, indicating its potential application in cold seasons or regions.

Table 3 compares the performance and applications of SFC with other materials. The table presents the utilization of β-FeOOH for superhydrophobic modification in cotton fabrics and other substrates over the past few years. The existing modified materials can primarily be applied in oil/water separation but lack potential applications in textiles. In contrast, this study highlights the advantages of using β-FeOOH and PDMS-modified cotton fabric for oil/water separation, UV protection, photothermal conversion, anti-icing, and photothermal de-icing. Moreover, the SFC prepared in this study maintains the original breathability of cotton fabric, which is crucial for its application in textiles. The significant comparison results in Table 3 underscore the superior performance and application advantages of SFC, showcasing the significance of this work.

## Conclusions

This study introduces an economical, environmentally friendly, and efficient approach for fabricating superhydrophobic cotton fabric using $FeCl_3 \cdot 6H_2O$ and PDMS. SEM and AFM analysis revealed the presence of numerous nanoparticles in SFC, enhancing surface

**Table 3** Comparison of performance and application between SFC and other superhydrophobic modified materials

| Materials | Breathability | Self-cleaning | Anti-fouling | UV-blocking | Photothermal de-icing | Oil/water separation | Ref. |
|---|---|---|---|---|---|---|---|
| ***Cotton fabric*** | | | | | | | |
| β-FeOOH, PDMS | ☑ | ☑ | ☑ | ☑ | ☑ | ☑ | This work |
| β-FeOOH, PDA, DDT | ☒ | ☒ | ☒ | ☒ | ☒ | ☑ | (Cheng et al. 2020) |
| β-FeOOH, $NaNO_2$, $C_8H_5F_6N$ | ☒ | ☑ | ☒ | ☒ | ☒ | ☑ | (Li et al. 2021a) |
| β-FeOOH, SDS, urea | ☒ | ☒ | ☒ | ☒ | ☒ | ☑ | (Xue et al. 2019) |
| PDMS, STA, TEOS | ☒ | ☒ | ☒ | ☒ | ☒ | ☑ | (Tang and Liu 2023) |
| PDMS, Ag NPs | ☒ | ☑ | ☒ | ☑ | ☑ | ☒ | (Pakdel et al. 2023) |
| PDMS, Ti-MOFs | ☒ | ☑ | ☒ | ☑ | ☒ | ☑ | (Yang et al. 2019) |
| $TiO_2$, APTES, MA | ☒ | ☑ | ☑ | ☑ | ☒ | ☑ | (Ahmad et al. 2023) |
| RA, $SiO_2$, octenyl-POSS | ☒ | ☑ | ☑ | ☒ | ☒ | ☑ | (Chen et al. 2022) |
| $NH_2$-POSS, TA | ☒ | ☑ | ☑ | ☒ | ☒ | ☑ | (Shang et al. 2021) |
| ***Others*** | | | | | | | |
| γ-FeOOH, PDA, silk | ☒ | ☑ | ☒ | ☑ | ☒ | ☑ | (Zhou et al. 2020a) |
| β-FeOOH, BT, glutaraldehyde, 1-dodecanethiol, foam | ☒ | ☒ | ☒ | ☒ | ☒ | ☑ | (Chen et al. 2018) |
| β-FeOOH, Cu mesh, hydrophobic radicals | ☒ | ☑ | ☒ | ☒ | ☒ | ☑ | (Li et al. 2021b) |

roughness. FTIR-ATR, XPS, and XRD confirmed the chemical composition of SFC, indicating successful modification. SFC exhibited outstanding breathability, self-cleaning, and anti-fouling capabilities, maintaining superhydrophobicity even after exposure to strong acids, bases, and various organic solvents for 24 h. The CA of SFC remained above 150°after 600 min of standard water washing and 30 cycles of sandpaper abrasion tests, indicating robust durability.

Furthermore, SFC performed exceptionally well in UV-blocking, anti-icing, and photothermal de-icing. With a UPF value nearing 80, SFC proved an excellent UV-blocking material. Moreover, SFC exhibited efficacy in oil/water separation. This work provides new ideas for developing self-cleaning, anti-fouling, UV-blocking, anti-icing, photothermal de-icing, and brightly colored fabrics, showing attractive prospects in terms of cost, efficiency, and versatility in preparation.

**Author contributions** Hua-Bin Yuan: Investigation, Methodology, Data curation, Formal analysis, Writing–original draft. Manman Zhao: Data curation, Formal analysis, Methodology. Xiaowei Zhu: Investigation, Validation, Methodology. Desheng Sha: Investigation, Methodology. Guoqiang Chen: Supervision, Resources. Tieling Xing: Resources, Supervision, Conceptualization, Formal analysis, Writing–review & editing.

**Funding** This work was supported by the National Natural Science Foundation of China (51973144, 51741301); the Foundation of Jiangsu Engineering Research Center of Textile Dyeing and Printing for Energy Conservation, Discharge Reduction and Cleaner Production (ERC-Q811580722); the Priority Academic Program Development (PAPD) of Jiangsu Higher Education Institutions for Textile Engineering in Soochow University.

**Data availability** All the required data has been mentioned in the study.

**Declarations**

**Ethical approval** Not applicable.

**Competing interests** The authors declare no competing interests.

## References

Ahmad N, Rasheed S, Ahmed K et al (2023) Facile two-step functionalization of multifunctional superhydrophobic cotton fabric for UV-blocking, self cleaning, antibacterial, and oil-water separation. Sep Purif Technol 306:122626. https://doi.org/10.1016/j.seppur.2022.122626

Arumugam V, Kanthapazham R, Zherebtsov DA et al (2021) Fluorine free $TiO_2$/cyanate ester coated cotton fabric with low surface free energy and rough surface for durable oil–water separation. Cellulose 28:4847–4863. https://doi.org/10.1007/s10570-021-03822-w

Bayer IS (2020) Superhydrophobic coatings from ecofriendly materials and processes: A review. Adv Mater Interfaces 7:2000095. https://doi.org/10.1002/admi.202000095

Chen C, Li Z, Hu Y et al (2022) Rosin acid and $SiO_2$ modified cotton fabric to prepare fluorine-free durable superhydrophobic coating for oil-water separation. J Hazard Mater 440:129797. https://doi.org/10.1016/j.jhazmat.2022.129797

Chen G, Cao Y, Ke L et al (2018) Plant polyphenols as multifunctional platforms to fabricate three-dimensional superhydrophobic foams for oil/water and emulsion separation. Ind Eng Chem Res 57:16442–16450. https://doi.org/10.1021/acs.iecr.8b03953

Chen J, Yuan L, Shi C et al (2021) Nature-inspired hierarchical protrusion structure construction for washable and wear-resistant superhydrophobic textiles with self-cleaning ability. ACS Appl Mater Interfaces 13:18142–18151. https://doi.org/10.1021/acsami.1c03539

Chen T, Hong J, Peng C et al (2019) Superhydrophobic and flame retardant cotton modified with DOPO and fluorine-silicon-containing crosslinked polymer. Carbohydr Polym 208:14–21. https://doi.org/10.1016/j.carbpol.2018.12.023

Cheng D, Zhang Y, Bai X et al (2020) Mussel-inspired fabrication of superhydrophobic cotton fabric for oil/water separation and visible light photocatalytic. Cellulose 27:5421–5433. https://doi.org/10.1007/s10570-020-03149-y

Cheng Q-Y, Zhao X-L, Weng Y-X et al (2019) Fully Sustainable, nanoparticle-free, fluorine-free, and robust superhydrophobic cotton fabric fabricated via an eco-friendly method for efficient oil/water separation. ACS Sustainable Chem Eng 7:15696–15705. https://doi.org/10.1021/acssuschemeng.9b03852

Chung C, Lee M, Choe EK (2004) Characterization of cotton fabric scouring by FT-IR ATR spectroscopy. Carbohydr Polym 58:417–420. https://doi.org/10.1016/j.carbpol.2004.08.005

Emam HE, Darwesh OM, Abdelhameed RM (2020) Protective cotton textiles via amalgamation of cross-linked zeolitic imidazole frameworks. Ind Eng Chem Res 59:10931–10944. https://doi.org/10.1021/acs.iecr.0c01384

Gu J, Yan X, Qi D et al (2022) Fabrication of durable coatings for cotton fabrics with flame retardant, antibacterial, fluorine-free superhydrophobic and self-cleaning properties. Cellulose. https://doi.org/10.1007/s10570-022-04892-0

Guo W, Wang X, Huang J et al (2020) Construction of durable flame-retardant and robust superhydrophobic coatings on cotton fabrics for water-oil separation application. Chem Eng J 398:125661. https://doi.org/10.1016/j.cej.2020.125661

Hu Z, Li W (2012) Preparation of superhydrophobic $Fe_2O_3$ nanorod films with the tunable water adhesion. J Colloid Interface Sci 376:245–249. https://doi.org/10.1016/j.jcis.2012.01.023

Jiang Y-H, Zhang Y-Q, Wang Z-H et al (2022) Controllable construction of multifunctional superhydrophobic coating with ultra-stable efficiency for oily water treatment. J Colloid Interface Sci 628:356–365. https://doi.org/10.1016/j.jcis.2022.07.143

Li W, Wang X, Wu Y et al (2021a) One-step spontaneous grafting via diazonium chemistry for the fabrication of robust bionic multifunctional superhydrophobic fabric. Surf Coat Technol 407:126802. https://doi.org/10.1016/j.surfcoat.2020.126802

Li W, Xi Y, Li Z (2021b) Anisotropic overgrowth of metal heterostructures regulated by a hydrophobic grafting layer towards self-cleaning and oil/water separation applications. Surf Coat Technol Technology 427:127814. https://doi.org/10.1016/j.surfcoat.2021.127814

Li W, Zhang Y, Yu Z et al (2022) In Situ Growth of a stable metal–organic framework (MOF) on flexible fabric via a layer-by-layer strategy for versatile applications. ACS Nano 16:14779–14791. https://doi.org/10.1021/acsnano.2c05624

Ling Z, Wang T, Makarem M et al (2019) Effects of ball milling on the structure of cotton cellulose. Cellulose 26:305–328. https://doi.org/10.1007/s10570-018-02230-x

Liu J, Xiong J, Huang Q et al (2022) Eco-friendly synthesis of robust bioinspired cotton fabric with hybrid wettability for integrated water harvesting and water purification. J Cleaner Prod 350:131524. https://doi.org/10.1016/j.jclepro.2022.131524

Liu L, Ma Z, Zhu M et al (2023) Superhydrophobic self-extinguishing cotton fabrics for electromagnetic interference shielding and human motion detection. J Mater Sci Technol 132:59–68. https://doi.org/10.1016/j.jmst.2022.05.036

Liu Q, Wu Y, Li Z (2020) Facile preparation of super-hydrophobic fabrics composed of fibres with microporous or microspherical coatings using the static breath figure method. Prog Org Coat 149:105938. https://doi.org/10.1016/j.porgcoat.2020.105938

Mohamed ME, Abd-El-Nabey BA (2021) Fabrication of durable superhydrophobic/oleophilic cotton fabric for highly efficient oil/water separation. Water Sci Technol 83:90–99. https://doi.org/10.2166/wst.2020.562

Pakdel E, Sharp J, Kashi S et al (2023) Antibacterial superhydrophobic cotton fabric with photothermal, self-cleaning, and ultraviolet protection functionalities. ACS Appl Mater Interfaces 15:34031–34043. https://doi.org/10.1021/acsami.3c04598

Shang Q, Hu L, Yang X et al (2021) Superhydrophobic cotton fabric coated with tannic acid/polyhedral oligomeric silsesquioxane for highly effective oil/water separation. Prog Org Coat 154:106191. https://doi.org/10.1016/j.porgcoat.2021.106191

Sharma U, Pandey R, Basu S, Saravanan P (2023) ZIF-67 blended PVDF membrane for improved Congo red removal and antifouling properties: a correlation establishment between morphological features and ultra-filtration parameters. Chemosphere 320:138075. https://doi.org/10.1016/j.chemosphere.2023.138075

Tang D, Liu E (2023) Facile fabrication of robust and fluorine-free superhydrophobic PDMS/STA-coated cotton fabric for highly efficient oil-water separation. Coatings 13:954. https://doi.org/10.3390/coatings13050954

Wang S, Li D, Zhou Y, Jiang L (2020) Hierarchical $Ti_3C_2T_x$ MXene/Ni chain/ZnO array hybrid nanostructures on cotton fabric for durable self-cleaning and enhanced microwave absorption. ACS Nano 14:8634–8645. https://doi.org/10.1021/acsnano.0c03013

Wu M, Ma B, Pan T et al (2016) Silver-nanoparticle-colored cotton fabrics with tunable colors and durable antibacterial and self-healing superhydrophobic properties. Adv Funct Mater 26:569–576. https://doi.org/10.1002/adfm.201504197

Xie H, Chen B, Lin H et al (2023) Efficient oil-water emulsion treatment via novel composite membranes fabricated by $CaCO_3$-based biomineralization and TA-Ti(IV) coating strategy. Sci Total Environ 857:159183. https://doi.org/10.1016/j.scitotenv.2022.159183

Xiong M, Ren Z, Liu W (2020) Fabrication of superhydrophobic and UV-resistant surface on cotton fabric via layer-by-layer assembly of silica-based UV absorber. J Dispersion Sci Technol 41:1703–1710. https://doi.org/10.1080/01932691.2019.1634589

Xue S, Xu X, Zhang L (2019) Fabrication of ecofriendly recycled marimo-like hierarchical micronanostructure superhydrophobic materials for effective and selective separation of oily pollutants from water. Ind Eng Chem Res 58:5613–5621. https://doi.org/10.1021/acs.iecr.8b06411

Yang R, Liu B, Yu F et al (2023) Superhydrophobic cellulose paper with sustained antibacterial activity prepared by in-situ growth of carvacrol-loaded zinc-based metal organic framework nanorods for food packaging application. Int J Biol Macromol 234:123712. https://doi.org/10.1016/j.ijbiomac.2023.123712

Yang Y, Huang W, Guo Z et al (2019) Robust fluorine-free colorful superhydrophobic PDMS/$NH_2$-MIL-125(Ti)@cotton fabrics for improved ultraviolet resistance and efficient oil–water separation. Cellulose 26:9335–9348. https://doi.org/10.1007/s10570-019-02707-3

Yuan H-B, Zhao M, Lei X et al (2024) Fabrication of multifunctional cotton fabric with “pompon mum” shaped surface by ZIF-8 for applications in oil-water separation and anti-icing. Prog Org Coat 186:108056. https://doi.org/10.1016/j.porgcoat.2023.108056

Żebrowska K, Coy E, Synoradzki K et al (2020) Facile and controllable growth of β-FeOOH nanostructures on polydopamine spheres. J Phys Chem B 124:9456–9463. https://doi.org/10.1021/acs.jpcb.0c06627

Zhang G, Liu Y, Chen C et al (2022) MOF-based cotton fabrics with switchable superwettability for oil–water separation. Chem Eng Sci 256:117695. https://doi.org/10.1016/j.ces.2022.117695

Zhang M, Wang S, Wang C, Li J (2012) A facile method to fabricate superhydrophobic cotton fabrics. Appl Surf Sci 261:561–566. https://doi.org/10.1016/j.apsusc.2012.08.055

Zhou M, Zhang L, Zhong L, et al (2023) Robust photothermal icephobic surface with mechanical durability of multi-bioinspired structures. Adv Mater n/a:2305322. https://doi.org/10.1002/adma.202305322

Zhang S, Fang K, Liu X et al (2023) Enhancement UV-resistance and hydrophobic of cotton fabrics through membrane formation by cationic colored nanospheres. Surf Interfaces 37:102701. https://doi.org/10.1016/j.surfin.2023.102701

Zhao Q, Wu LYL, Huang H, Liu Y (2016) Ambient-curable superhydrophobic fabric coating prepared by water-based non-fluorinated formulation. Mater Des 92:541–545. https://doi.org/10.1016/j.matdes.2015.12.054

Zhou Q, Chen G, Xing T (2018) Facile construction of robust superhydrophobic tea polyphenol/Fe@cotton

fabric for self-cleaning and efficient oil–water separation. Cellulose 25:1513–1525. https://doi.org/10.1007/s10570-018-1654-1

Zhou Q, Wu W, Zhou S et al (2020a) Polydopamine-induced growth of mineralized γ-FeOOH nanorods for construction of silk fabric with excellent superhydrophobicity, flame retardancy and UV resistance. Chem Eng J 382:122988. https://doi.org/10.1016/j.cej.2019.122988

Zhou Y, Ma Y, Sun Y et al (2020b) Facile preparation of robust superhydrophobic cotton fabric for ultrafast removal of oil from contaminated waters. Environ Sci Pollut Res 27:21202–21212. https://doi.org/10.1007/s11356-020-08209-1